Electrical Signature of the Percolation Threshold in Sea Ice

Kenneth M. Golden, Hajo Eicken, Adam Gully, Malcolm Ingham, Keleigh A. Jones, Joyce Lin, James E. Reid, Christian S. Sampson, and Anthony P. Worby

February 1, 2021

Abstract

Fluid flow through sea ice governs a broad range of geophysical and biological processes in the polar marine environment. For example, the evolution of melt ponds and sea ice albedo, which is important in climate modeling, is constrained by drainage through the porous brine microstructure. However, for brine volume fractions below about 5%, columnar sea ice is effectively impermeable to fluid flow. In two different experiments conducted in the Arctic and Antarctic, we have found that this critical fluid transition exhibits a strong electrical signature, with sea ice resistivity rising sharply over three orders of magnitude near the brine connectivity threshold. The data are accurately explained by percolation theory, with the same universal critical exponent which captures fluid permeability. These results enable us to connect specific electrical profiles to important transport processes such as melt pond drainage, CO_2 pumping, and the flux of nutrients which sustain biomass build-up.

1 Introduction

Polar sea ice is a key component of Earth's climate system, and a leading indicator of climate change [33, 30]. As a material sea ice is a composite of pure ice with brine and air inclusions. The brine phase hosts extensive microbial communities which sustain life in the polar oceans [33, 10]. Fluid flow through the porous microstructure mediates key processes impacting the climatology and biology of sea ice. Improving projections of the fate of Earth's sea ice cover and its ecosystems depends on a better understanding of these important processes and feedback mechanisms.

For example, the evolution of sea ice albedo represents a fundamental problem in climate modeling and a significant source of uncertainty in climate projections [7, 24]. The albedo of sea ice floes is determined by melt pond evolution [22, 24]. Drainage of the ponds, with a resulting increase in albedo, is largely

controlled by the fluid permeability of the porous sea ice underlying the ponds [6, 14]. As ice recedes with melting, more water surface is exposed, which increases solar absorption, leading in turn to more melting, and so on. This *ice–albedo feedback* has played a significant role in the decline of the summer Arctic ice pack [23].

Fluid flow through sea ice governs the evolution of the salt budget and salinity profiles [33], convection-enhanced thermal transport [20], ocean-ice-atmosphere CO_2 exchanges [27], and the build-up of algal biomass fueled by nutrient fluxes [33, 10]. It also drives snow-ice formation, accounting for a significant portion of the ice produced in the Southern Ocean [21]. Sea water percolates upward through the porous microstructure, flooding the snow layer, and subsequently freezing.

While fluid flow is substantially restricted for brine volume fractions ϕ below about 5%, columnar sea ice is increasingly permeable for ϕ above 5% [13]. For a typical bulk salinity of 5 ppt, the critical porosity $\phi_c \approx 5\%$ corresponds to a temperature $T_c \approx -5^\circ$ C, which is known as the *rule of fives*. This critical behavior of the fluid permeability results from a connectivity or percolation threshold in the brine microstructure [13, 14, 25].

If the fluid transport properties of sea ice can be linked to its electrical properties, which is the aim of this paper, then new approaches can be brought to bear in monitoring the state of sea ice. For example, it could open the door to the development of sensors to enhance existing buoy networks, provide information on key ice processes, and improve integration with satellite data.

The electrical conductivity of sea ice has been studied over the past five decades [1, 3, 11, 17, 26, 34]. However, there have been no observations of critical behavior in electrical properties corresponding to the microstructural transition encapsulated in the rule of fives. Here we report on two types of experiments where electrical resistivity data clearly display critical behavior at the brine percolation threshold. The mathematical description we develop provides a rigorous link between fluid and electrical transport in sea ice, with both displaying the same type of universal critical behavior, thus laying the foundation for the techniques referred to above. In fact, we further develop this foundation by partitioning the range of resistivity values of our data into intervals which correspond to distinct regimes of fluid permeability characteristics and related process behavior, such as melt pond development, and fluxes of nutrients and CO_2.

One of the goals of this work is to obtain data on the linkages between electrical and hydraulic properties [35]. The value of such an approach lies in the potential to then extract information about other key variables describing the state of sea ice, e.g., pertaining to its rheology or potential to harbor microbial communities. Our results indicate that such information could potentially be obtained from measurements of electric properties via *in situ* drifting sensors that can monitor the evolution of sea ice nondestructively (Figure 1 d).

The findings presented here also have implications for measuring ice thickness, an important gauge of the impact of global warming. Not only are thickness data important in comparing climate model predictions to observed behav-

ior, but in specifying the initial conditions necessary for long-term numerical simulations. Promising techniques for advanced airborne or surface-based measurements of ice thickness depend on the interaction of electromagnetic (EM) fields with sea ice. For example, there has been significant interest in the development of EM induction devices [15, 26] mounted on ships, planes and helicopters. These techniques, and the interpretation of the data to obtain thickness information, rely on knowledge of the electrical properties of sea ice, and how they vary with depth, temperature, salinity, and ice type. The results presented here shed significant light on such issues.

2 Measuring the Electrical Properties of Sea Ice

Sea ice is an anisotropic composite with vertically elongated brine inclusions and corresponding anisotropy in the effective fluid permeability and electrical conductivity tensors. Most methods for measuring sea ice conductivity involve indirect or inverse techniques, such as surface-based geoelectric profiling using a Wenner array of electrodes [3, 11, 17, 26, 29, 34]. Generally with these methods the vertical conductivity σ_v^* is inherently mixed with the horizontal components. Here we are most interested in σ_v^* due to its connection with vertical fluid flow.

During the Sea Ice Physics and Ecosystem Experiment (SIPEX) in September and October of 2007, we made *direct* measurements of σ_v^* in Antarctic pack ice by adapting a four probe Wenner array for use in cylindrical ice cores, as shown in Figure 1 a and b. The study area was located off the coast of East Antarctica, between 115° E and 130° E, and 64° S and 66° S. At 8 of the 15 ice stations along the cruise track of the Australian icebreaker *Aurora Australis*, we extracted vertical cores from thin first-year sea ice, with lengths ranging from 34 cm to 86 cm. Thermistor probes were inserted into small holes drilled every 5 cm. We used a Wenner electrode array along sections of the cores, connected to a YEW Earth Resistance Tester operating at 38 Hz. This set-up yields the resistance along the axis of the cylindrical ice core between probes P1 and P2, corresponding to the vertical direction *in situ*, with $a = L = 10$ cm (or $a = L = 5$ cm in some cases). We obtained 26 averaged data points from 67 raw measurements of the resistance between the inner probes. After the temperature and resistance measurements were taken, which took about 10 to 20 minutes, we cut each core into 10 cm sections which were later melted, so that we could obtain bulk salinity measurements for each section. The temperature and salinity measurements allowed us to calculate a brine volume fraction profile for each core [5].

In the Arctic, we used the technique of cross-borehole DC resistivity tomography [17, 18], as shown in Figure 1 c and d. The ice is probed in its natural state, utilizing two or four vertical strings of electrodes frozen into the ice. It has been shown that this method can be used to derive the horizontal component of the anisotropic resistivity profile. Moreover, it has been demonstrated that the vertical component of $\boldsymbol{\sigma}^*$ can be obtained as well [17, 18]. If a minimum of four electrode strings are used, the geometric mean of the vertical and horizontal

components of $\boldsymbol{\sigma}^*$ can be derived, along with the horizontal component [17], yielding the vertical component.

Measurements of the temporal variation in the resistivity structure of first-year Arctic sea ice through spring warming have been made approximately 1 km off the coast of Barrow, Alaska at 71° 21′ 56.45″ N, 156° 32′ 39.01″ W. Electrode strings were installed in landfast first year ice in late January 2008. Cross-borehole measurements were made on 6 separate occasions between early April and mid June 2008, allowing both the horizontal and vertical components of the ice resistivity to be derived. A sea ice mass balance site and an ice core sampling program at the same location [4] provided ice temperature and salinity data, allowing the variation in resistivity structure to be correlated with brine volume fraction ϕ.

Plate electrodes in contact with the ends of a cylinder generate parallel field lines which make measuring the conductivity of the cylinder material relatively straightforward. To assess the accuracy of our four probe method, the commercial package Comsol 3.5a was used to create a finite element model of cylindrical sea ice cores 0.09 m in diameter and 0.5 m in length. Four metal probes of 0.004 m in diameter and 0.09 m in length were inserted approximately 0.07 m into the core, similar to Figure 1 b. When the current is injected through the outer probes instead of parallel plates, the nearby field lines show significant curvature. However, in a boxed measurement region where the inner probes are located, the field lines are relatively straight, thus minimizing the error between the actual conductivity of the material and what is measured by the array. Numerical simulations show that if the outer probes are 5 cm or more from the inner measurement region, this error is less than 8.5%, and is less than 1.5% if the distance is 10 cm or more, as for much of our data. This is illustrated in Figure 2.

When extracting a sea ice core to measure its properties, loss of brine is a principal concern. However, for our experiments we did not see any evidence of significant brine loss during the relatively short measurement periods with air temperatures ranging from about −6° C to −18° C (with most below −9° C). Moreover, the probes are inserted deep into the core, minimizing contact with potential brine surface films. Our numerical simulations and these observations establish the Wenner array as a viable field method for *direct* resistivity measurements.

3 Modeling the Electrical Conductivity of Sea Ice

Lattice and continuum percolation theories [31] have been used to model a broad range of disordered materials where the connectedness of one phase dominates effective transport behavior. Consider the square ($d = 2$) or cubic ($d = 3$) network of bonds joining nearest neighbor sites on the integer lattice $\mathbb{Z}^d$. The bonds are assigned electrical conductivities $\sigma_0 > 0$ (open) or 0 (closed) with

probabilities p and $1-p$. Groups of connected open bonds are called open clusters, and the average cluster size grows as p increases. In this model there is a critical probability p_c, $0 < p_c < 1$, called the *percolation threshold*, where an infinite cluster of open bonds first appears. In $d = 2$, $p_c = \frac{1}{2}$, and in $d = 3$, $p_c \approx 0.25$. Typical configurations for the $d = 2$ square lattice above and below the threshold are shown in Figure 3. a and b.

Let $\sigma^*(p)$ be the effective conductivity of the network in the vertical direction [31]. For $p < p_c$, $\sigma^*(p) = 0$. For $p > p_c$ and near p_c, $\sigma^*(p)$ exhibits power law behavior,

$$\sigma^*(p) \sim \sigma_0 (p - p_c)^t \ , \quad p \to p_c^+, \tag{1}$$

where t is the conductivity critical exponent. For lattices, t is believed to be universal, depending only on d. In $d = 2$, $t \approx 1.3$, and in $d = 3$, $t \approx 2.0$ [31]. There is also a rigorous bound [12] that $1 \leq t \leq 2$ in $d = 2$ and $d = 3$. Since $\sigma^*(p) \to 0$ as $p \to p_c^+$, the effective resistivity $\rho^*(p) = 1/\sigma^*(p)$ diverges as $p \to p_c^+$, with a vertical asympote at $p = p_c$. For two phase composites with finite component resistivities, like sea ice, the behavior only approximates the asymptote, and for $p < p_c$, ρ^* remains finite.

The fluid permeability $\kappa^*(p)$ corresponding to (1), where the open bonds are pipes of fluid conductivity $\kappa_0/\eta = r_0^2/8\eta$ and radius r_0, behaves like $\kappa^*(p) \sim \kappa_0 (p - p_c)^e$ as $p \to p_c^+$, with e the fluid permeability exponent and η the fluid viscosity. For lattices, it is believed [31] that $e = t$. In the continuum, the exponents e and t can take non-universal values, and need not be equal, such as for the three dimensional Swiss cheese model [16, 31]. However, for lognormally distributed inclusions, as in sea ice, the behavior is *universal* [14, 2]. Thus for sea ice, $t = e \approx 2$.

In order to use percolation theory to quantitatively describe the vertical conductivity $\sigma_v^*(\phi)$, and to provide a link between fluid and electrical transport in sea ice, we recall our result [14] for the vertical fluid permeability

$$k_v^*(\phi) \ \sim \ 3 \ (\phi - \phi_c)^2 \ \times 10^{-8} \ \mathrm{m}^2, \quad \phi \to \phi_c^+. \tag{2}$$

The scaling factor $k_0 = 3 \times 10^{-8}$ is estimated using critical path analysis [31, 9]. The effective behavior of media with a broad range of local conductances is dominated by a critical *bottleneck* conductance related to the minimal radius in a connected pathway of appropriate scale. To relate σ_v^* to k_v^*, we use the following relation from critical path analysis [9]. With r_c denoting the critical radius for our centimeter scale electrical experiments, then

$$k_v^* = \frac{r_c^2}{8} \ \frac{\sigma_v^*}{\sigma_b} \ , \tag{3}$$

where σ_b is the conductivity of brine, which depends [32] on temperature T. By measuring the radii of vertical pathways in X-ray tomography images [14, 25], we estimate a range in mm of $0.1 \leq r_c \leq 0.2$.

It is useful to consider the vertical conductivity formation factor $F = \sigma_v^*/\sigma_b$, which removes the dependence of the effective parameter on the changing conductivity of the brine, and depends only on the pore volume fraction and geometry. In view of (1) and (3), $F(\phi) \ \sim \ F_0 \ (\phi - \phi_c)^2$ as $\phi \to \phi_c^+$, where

$F_0 = 8k_0/r_c^2$. The estimates of 0.1 mm to 0.2 mm for r_c yield a range for F_0 of $6 \leq F_0 \leq 24$.

In order to compare our conductivity measurements with percolation theory, we must exclude data below $\phi_c \approx 0.05$ [14], since the theory is only valid for $\phi > \phi_c$. It is more illustrative to display the data in terms of the reciprocal $G = 1/F = \rho_v^*/\rho_b$, which is the vertical resistivity formation factor. In Figure 3 c and d we show the two data sets from the Antarctic and Arctic. By fixing the exponent $t = 2$ and the threshold value $\phi_c = 0.05$ in the above expression for $F(\phi)$, a statistical best fit of the data yields a value of $F_0 \approx 9$, which lies inside our predicted range, so that

$$F(\phi) \ \sim \ 9\,(\phi - 0.05)^2, \quad \phi \to \phi_c^+. \tag{4}$$

We see that the data agree well with the theory, and that they both exhibit divergent behavior with a vertical asymptote at the percolation threshold. Moreover, in the variables $x = \log(\phi - 0.05)$ and $y = \log F$, the line predicted by percolation theory in (4) is $y = 2x + \log F_0$, with $\log F_0 = 0.95, F_0 = 9$. Critical path analysis yields the bounds $0.8 \leq \log F_0 \leq 1.4$, and the best fit for the Antarctic data in f is $y = 1.99x + 0.93$, where 0.93 lies inside these bounds. In logarithmic variables, the error of the regression is 0.38 for the Arctic data and 0.22 for the Antarctic data (that is, approximately 68% of the Antarctic data are within 0.22 of the regression line). The increased scatter in the Arctic data is not surprising given the inverse computation required to obtain the formation factor data.

To model $\sigma_v^*(\phi)$ over all porosities, we consider features of the brine phase present over the full range − some degree of small-scale connectivity, and self-similarity. Hierarchical models of spheres or other grains surrounded by smaller spheres, and so on, with brine in the pore spaces [14], were used to model $k_v^*(\phi)$. The simplest model yields a result of $k_v^*(\phi) = k_0\,\phi^3$. Via (3) we obtain an Archie's law result of $F(\phi) = F_0\,\phi^3$. A statistical best fit of our Antarctic data yields a value of $F_0 \approx 16$, which is in the estimated range. In Figure 4 a, our Antarctic data are shown along with fits derived from both models, and in b, Arctic permeability data [14] are shown relative to predictions from both models.

4 Discussion

Figure 5 illustrates how we can derive information about the permeability structure and relevant transport processes from resistivity soundings of Arctic sea ice with *in situ* electrode strings [18]. Thus, the different formation factor regimes shown correspond to different permeability classes, with the lowermost ice layers permeable enough to allow for gas and nutrient exchange conducive to biomass build-up and CO_2 pumping [19, 28], based on a critical permeability of 4×10^{-11} m^2, corresponding to a resistivity formation factor of 31.3 for $r_c = 0.1$ mm. This permeable base layer increases in vertical extent as the ice warms and thins due to bottom and surface melt. The ice interior is permeable enough to allow for

meltwater flushing and reduction of ice salinity at surface ablation rates of 10 cm/d or less even prior to the onset of melt [8], corresponding to a resistivity formation factor of 625. High resistivity formation factors near the top in Figure 5 b are in part explained by such percolation of freshwater below accumulations of surface melt water.

Let us further examine how our results may be used to provide a better understanding of key processes like melt pond evolution. Incorporating such processes into climate models is critical to improving projections of climate change. Development and tuning of improved climate models could be significantly enhanced by ground truth information and monitoring of these key processes and the internal state of the sea ice.

For example, there is recent evidence from Arctic sea ice experiments (conducted by C. Polashenski and K. M. Golden in 2014) that percolation of freshwater from snowmelt into the upper layers of sea ice, and its subsequent freezing, could be fundamental to the very formation of melt ponds. This process reduces the permeability − thus increasing the electrical resisitivity, a process likely to have a recognizable electrical signature, as evidenced in Figure 5. Gauging the impact, for example, of changing Arctic snowfall on the availability of freshwater for melt pond formation could be made possible with methods based on our results. Melt pond drainage events, which can have a significant impact on sea ice albedo, often follow an increase in permeability through its percolation threshold, which has a strong electrical signature. Specific information on electrical and fluid transport profiles would enable estimates of drainage rates, duration of events, and in conjunction with a ponding model (e.g., [6, 7]) provide insight into albedo changes. The resulting input of fresh water into the upper ocean is also an important process which may be tracked through in-ice sensors.

In the Antarctic, snow-ice formation is a significant component of sea ice production. Knowledge of the time evolution of the conductivity−permeability profile in Antarctic sea ice can help delineate regions and time periods conducive to snow-ice formation, e.g., to estimate snow-ice production during storm-driven snowfall events. Like melt ponds in the Arctic, incorporating snow-ice formation into Antarctic sea ice and climate models is critical to improving projections.

Laboratory and field work [19, 36] have demonstrated the importance of permeability changes in spring in driving a key seasonal transition associated with disproportionate increases in gas transfer, nutrient exchange and biological activity in sea ice. In [36] it was demonstrated how this important transition enhances primary production within the ice and under the ice through seeding of under-ice waters. Since there is no clear surface expression of these processes, *in situ* measurement of electrical conductivity (e.g., through arrays sampling large volumes [18]) may serve as an important proxy and help track changes in the timing and magnitude of seasonal increases in gas, nutrient and biomass transfer.

5 Conclusions

It has been demonstrated in field experiments conducted in both the Arctic and Antarctic that sea ice exhibits critical behavior in its electrical transport properties at a percolation threshold. Such behavior provides the electrical signature of a key transition in fluid transport properties, known as the *rule of fives*, which determines whether or not fluid can flow through sea ice. This transition constrains a broad range of processes which are important in the geophysics and biology of the polar regions. The phenomenon is explained theoretically using percolation theory, which provides a universal power law describing the data from both poles, as well as a rigorous link between the fluid and electrical transport properties of sea ice. Our findings open the door to a new generation of techniques for *in situ* analysis and remote monitoring of transport processes, which can improve projections of the fate of Earth's ice packs and the response of polar ecosystems.

6 Acknowledgments

We are grateful for the support provided by the Division of Mathematical Sciences (DMS), the Arctic Natural Sciences (ARC) Program, and the Office of Polar Programs (OPP) at the US National Science Foundation (NSF) through grants DMS-0537015, DMS-0940249, and ARC-0934721. Joyce Lin was supported by an NSF Postdoctoral Fellowship through a VIGRE grant (DMS-0602219) to the Department of Mathematics at the University of Utah. Adam Gully and Christian Sampson were partially supported by the NSF Research Experiences for Undergraduates (REU) Program through the VIGRE grant, and graduate support through VIGRE. This work was also supported in part by the Australian Government through the Antarctic Climate and Ecosystems Cooperative Research Centre. Finally, we thank the crew of the *Aurora Australis* for their help and support during the SIPEX Antarctic expedition.

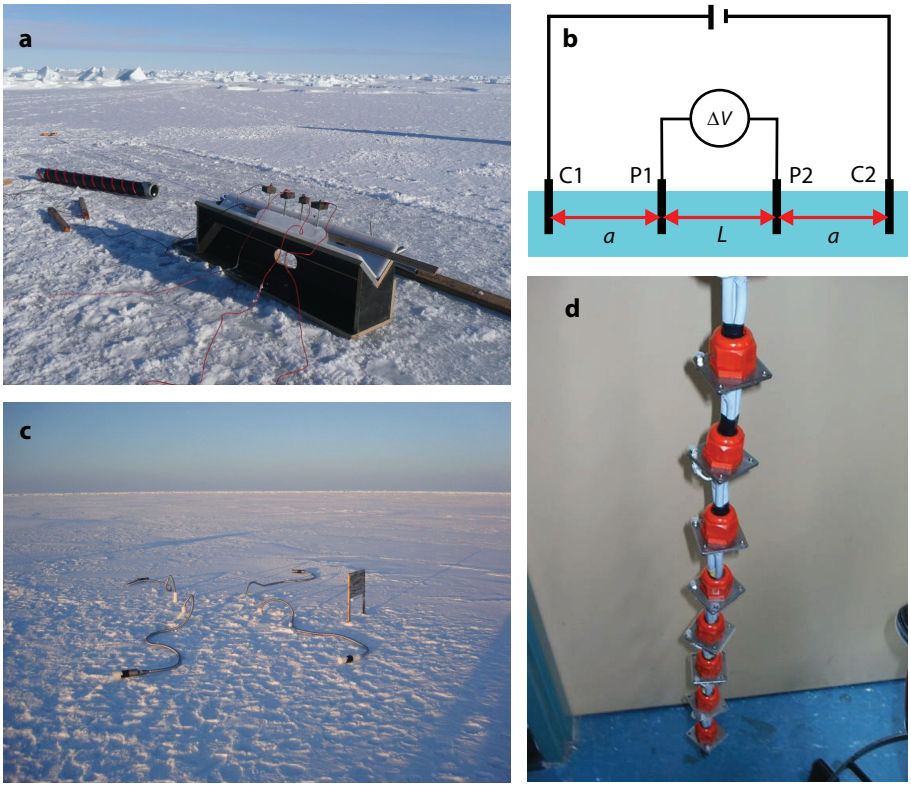

Figure 1: Examples of methods used to measure the conductivity the ice. (a) A Wenner electrode array is configured to measure the vertical conductivity of Antarctic sea ice, by inserting the four probes into an extracted ice core. (b) A current I is injected into the core through the outer electrodes C1 and C2. The potential difference ΔV resulting from the current flow is measured by the inner electrodes P1 and P2. The ratio $\Delta V/I$ is the resistance R in ohms. Here the electrode spacing is $L = 10$ cm and $a = 10$ cm. (c) A cross-borehole array is frozen into Arctic sea ice. The DC resistivity profile was tomographically reconstructed in the volume enclosed by the electrode strings. One of the strings, with 10 cm separation of the plates, is shown in (d).

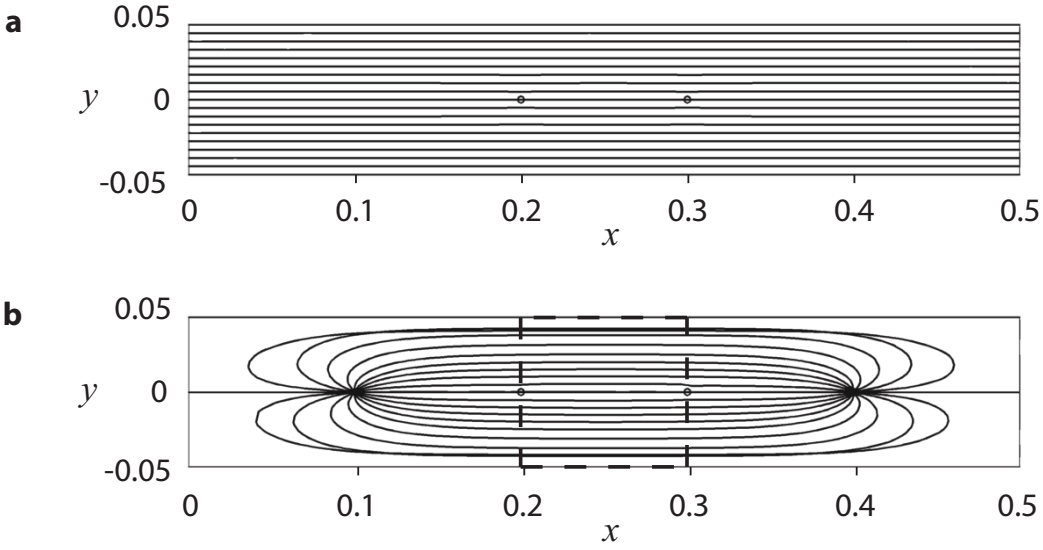

Figure 2: Comparing the field lines generated by parallel plates and a four probe Wenner array in sea ice. The field lines for a parallel plate configuration in (a) with those for a four probe Wenner array in vertically anisotropic ice (b).

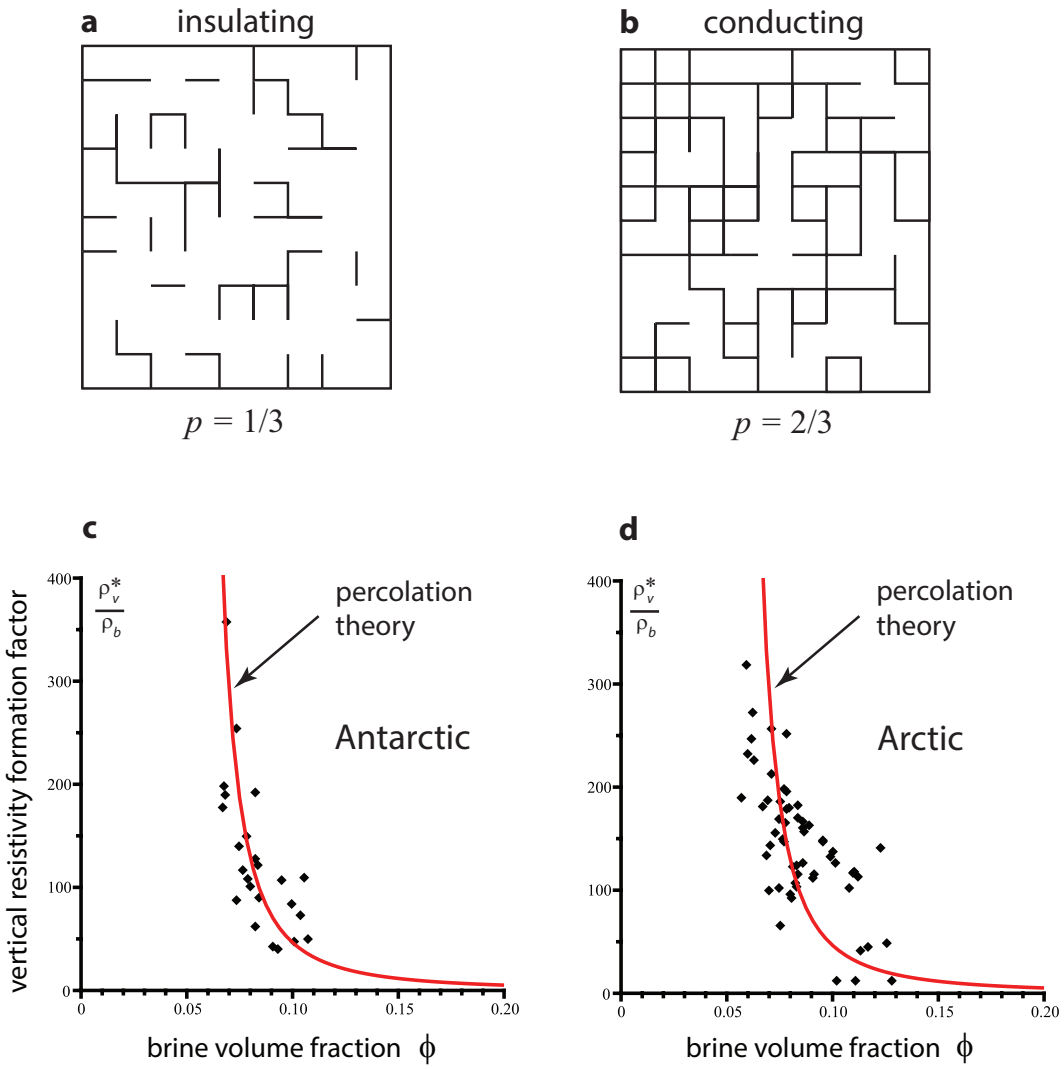

Figure 3: Examples of insulating and conducting two dimensional lattices and resistivity data from both the Arctic and Antarctic. The two dimensional square bond lattice below its percolation or connectivity threshold $p_c = 1/2$ in (a), and above in (b). We display the vertical resistivity formation factor data from the Antarctic in **(c)** and the Arctic in **(d)**, along with the same prediction from percolation theory in each. Both data and theory exhibit divergent behavior as ϕ approaches $\phi_c \approx 0.05$ from the right, with a vertical asymptote at $\phi = \phi_c$, electrically signaling the transition to relatively impermeable ice.

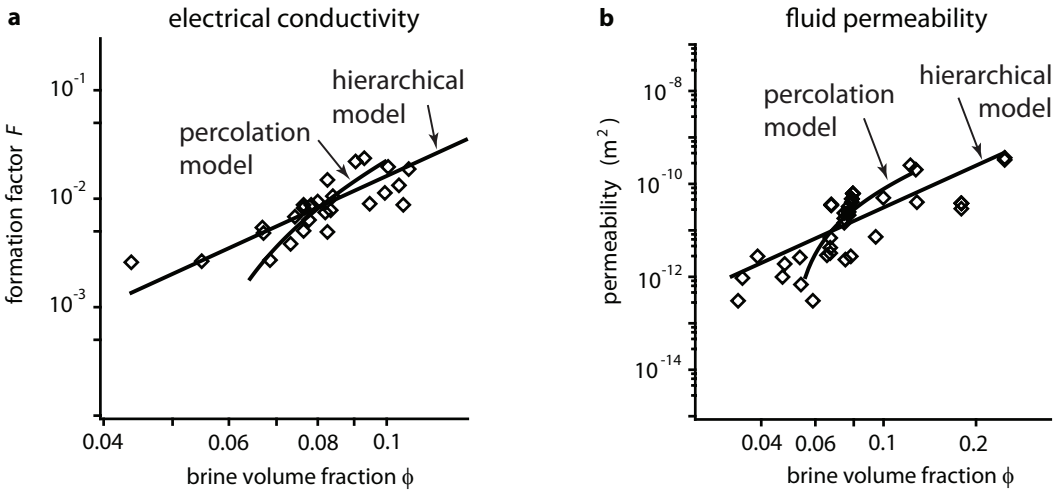

Figure 4: Antarctic conductivity data and Arctic fluid permeability data compared to percolation theory and the hierarchical model. (a) Antarctic field data on the vertical formation factor $F = \sigma_v^*/\sigma_b$ is compared with the hierarchical model $F(\phi) = F_0\phi^3$. The prediction of percolation theory is also shown. (B) Comparison of Arctic fluid permeability data with the hierarchical model, along with percolation theory [14]. In both figures percolation theory captures the trend of the data in the percolation regime more closely than Archie's law.

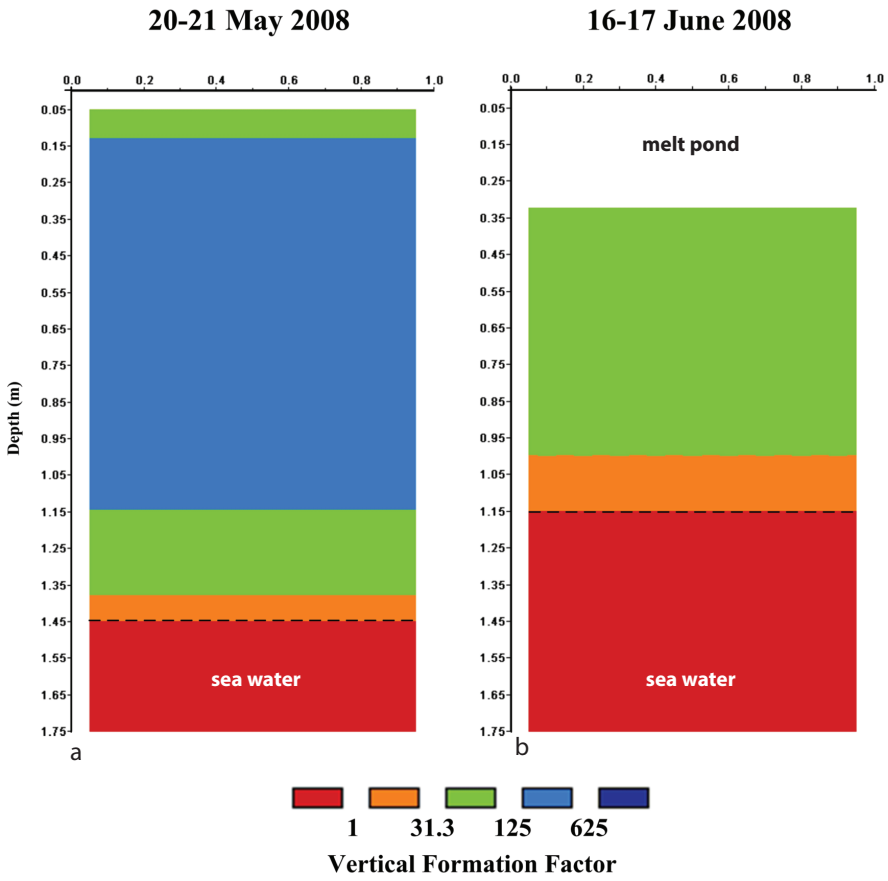

Figure 5: Cross-borehole tomographic reconstructions of the vertical resistivity formation factor for Arctic sea ice. We show in (a) the profile before melt pond formation, and (b) after. The evolution of resistivity structure is consistent with warming of the ice, thus increasing the fluid permeability and facilitating the infiltration of meltwater into the upper layer of sea ice from the surface. To connect the electrical properties of sea ice to its important processes, the range of the resistivity formation factor G is divided into five regimes: $G > 625$ (ice impermeable enough to allow ponds to grow for surface ablation rates 10 cm/d or larger for a critical pore radius of 0.1 mm); $125 < G \leq 625$, blue (ice impermeable enough to allow ponds to grow for surface ablation rates between 10 and 50 cm/d for a critical pore radius of 0.1 mm); $31.3 < G \leq 125$, green (at formation factors of 31.3 or larger ice is impermeable from the perspective of CO_2 exchange and build-up of nutrients and biomass in the ice [28], and sufficiently impermeable to drainage to support surface ponding); $1 < G \leq 31.3$, orange (highly permeable ice that allows for CO_2 pumping and build-up of nutrients and biomass); $G \leq 1$, red (assumed to be free water column). Only the most resistive ice $G > 625$ is not shown.

References

[1] J. Addison. Electrical properties of saline ice. *J. Appl. Phys.*, 40:3105–3114, 1969.

[2] B. Berkowitz and I. Balberg. Percolation approach to the problem of hydraulic conductvity in porous media. *Transport in Porous Media*, 9:275–286, 1992.

[3] R. G. Buckley, M. P. Staines, and W. H. Robinson. In situ measurements of the resistivity of Antarctic sea ice. *Cold Reg. Sci. Technol.*, 12(3):285–290, 1986.

[4] M. L. Druckenmiller, H. Eicken, M. A. Johnson, D. J. Pringle, and C. C. Williams. Towards an integrated coastal sea-ice observatory: System components and a case study at Barrow, Alaska. *Cold Reg. Sci. Technol.*, 56:61–72, 2009.

[5] H. Eicken. Growth, microstructure and properties of sea ice. In D. N. Thomas and G. S. Dieckmann, editors, *Sea Ice: An Introduction to its Physics, Chemistry, Biology and Geology*, pages 22–81. Blackwell, Oxford, 2003.

[6] H. Eicken, T. C. Grenfell, D. K. Perovich, J. A. Richter-Menge, and K. Frey. Hydraulic controls of summer Arctic pack ice albedo. *J. Geophys. Res. (Oceans)*, 109(C18):C08007.1–C08007.12, 2004.

[7] D. Flocco, D. L. Feltham, and A. K. Turner. Incorporation of a physically based melt pond scheme into the sea ice component of a climate model. *J. Geophys. Res.*, 115:C08012 (14 pp.), doi:10.1029/2009JC005568, 2010.

[8] J. Freitag and H. Eicken. Meltwater circulation and permeability of Arctic summer sea ice derived from hydrological field experiments. *J. Glaciol.*, 49:349–358, 2003.

[9] A. P. Friedman and N. A. Seaton. Critical path analysis of the relationship between permeability and electrical conductivity of three-dimensional pore networks. *Water Resources Res.*, 34(7):1703–1710, 1998.

[10] C. H. Fritsen, V. I. Lytle, S. F. Ackley, and C. W. Sullivan. Autumn bloom of Antarctic pack-ice algae. *Science*, 266:782–784, 1994.

[11] K. Fujino and Y. Suzuki. An attempt to estimate the thickness of sea ice by electrical resistivity method ii. *Low Temp. Sci.*, A21:151–157, 1963.

[12] K. Golden. Convexity and exponent inequalities for conduction near percolation. *Phys. Rev. Lett.*, 65(24):2923–2926, 1990.

[13] K. M. Golden, S. F. Ackley, and V. I. Lytle. The percolation phase transition in sea ice. *Science*, 282:2238–2241, 1998.

[14] K. M. Golden, H. Eicken, A. L. Heaton, J. Miner, D. Pringle, and J. Zhu. Thermal evolution of permeability and microstructure in sea ice. *Geophys. Res. Lett.*, 34:L16501 (6 pages and issue cover), doi:10.1029/2007GL030447, 2007.

[15] C. Haas. Late-summer sea ice thickness variability in the Arctic Transpolar Drift 1991-2001 derived from ground-based electromagnetic sounding. *Geophys. Res. Lett.*, 31:L09402, doi:10.1029/2007GL030447, 2004.

[16] B. I. Halperin, S. Feng, and P. N. Sen. Differences between lattice and continuum percolation transport exponents. *Phys. Rev. Lett.*, 54(22):2391–2394, 1985.

[17] M. Ingham, D. J. Pringle, and H. Eicken. Cross-borehole resistivity tomography of sea ice. *Cold Reg. Sci. Technol.*, 52:263–277, 10.1016/jcoldregions.2007.05.002, 2008.

[18] K. A. Jones, M. Ingham, D. J. Pringle, and H. Eicken. Temporal variations in sea ice resistivity: Resolving anisotropic microstructure through cross-borehole dc resistivity tomography. *J. Geophys. Res.*, 115:C11023, doi:10.1029/2009JC006049, 2010.

[19] Brice Loose, Lisa Miller, Scott Elliot, and Timothy Papakyriakou. Sea ice biogeochemistry and material transport across the frozen interface. *Oceanography*, 24(3):202–218, sep 2011.

[20] V. I. Lytle and S. F. Ackley. Heat flux through sea ice in the Western Weddell Sea: Convective and conductive transfer processes. *J. Geophys. Res.*, 101(C4):8853–8868, 1996.

[21] T. Maksym and T. Markus. Antarctic sea ice thickness and snow-to-ice conversion from atmospheric reanalysis and passive microwave snow depth. *J. Geophys. Res.*, 113:C02S12, doi:10.1029/2006JC004085, 2008.

[22] D. K. Perovich, T. C. Grenfell, B. Light, and P. V. Hobbs. Seasonal evolution of the albedo of multiyear Arctic sea ice. *J. Geophys. Res. (Oceans)*, 107(C10):8044, doi:10.1029/2000JC000438, 2002.

[23] D. K. Perovich, B. Light, H. Eicken, K. F. Jones, K. Runciman, and S. V. Nghiem. Increasing solar heating of the Arctic Ocean and adjacent seas, 1979-2005: Attribution and role in the ice-albedo feedback. *Geophys. Res. Lett.*, 34:L19505, doi:10.1029/2007GL031480, 2007.

[24] C. Polashenski, D. Perovich, and Z. Courville. The mechanisms of sea ice melt pond formation and evolution. *J. Geophys. Res. C (Oceans)*, 117:C01001 (23 pp.), doi:10.1029/2011JC007231, 2012.

[25] D. J. Pringle, J. E. Miner, H. Eicken, and K. M. Golden. Pore-space percolation in sea ice single crystals. *J. Geophys. Res. (Oceans)*, 114:C12017, 12 pp., doi:10.1029/2008JC005145, 2009.

[26] J. E. Reid, A. Pfaffling, A. P. Worby, and J. R. Bishop. In situ measurements of the direct-current conductivity of Antarctic sea ice: Implications for airborne electromagnetic sounding of sea-ice thickness. *Ann. Glaciol.*, 44:217–223, 2006.

[27] S. Rysgaard, J. Bendtsen, L. T. Pedersen, H. Ramløv, and R. N. Glud. Increased CO_2 uptake due to sea ice growth and decay in the Nordic Seas. *J. Geophys. Res.*, 114:C09011, doi:10.1029/2008JC005088, 2009.

[28] S. Rysgaard, R. N. Glud, M. K. Sejr, J. Bendtsen, and P. B. Christensen. Inorganic carbon transport during sea ice growth and decay: A carbon pump in polar seas. *J. Geophys. Res.*, 112:C03016, doi:10.1029/ 2006JC003572, 2007.

[29] C. Sampson, K. M. Golden, A. Gully, and A. P. Worby. Surface impedance tomography for Antarctic sea ice. *Deep Sea Res. II*, 58:1149–1157, 2011.

[30] M. C. Serreze, M. M. Holland, and J. Stroeve. Perspectives on the Arctic's shrinking sea-ice cover. *Science*, 315:1533–1536, 2007.

[31] D. Stauffer and A. Aharony. *Introduction to Percolation Theory, Second Edition*. Taylor and Francis Ltd., London, 1992.

[32] A. Stogryn and G. J. Desargant. The dielectric properties of brine in sea ice at microwave frequencies. *IEEE Trans. Antennas Propagat.*, AP-33(5):523–532, 1985.

[33] D. N. Thomas and G. S. Dieckmann, editors. *Sea Ice, 2nd Edition*. Wiley-Blackwell, Oxford, 2009.

[34] F. Thyssen, H. Kohnen, M. V. Cowan, and G. W. Timco. DC resistivity measurements on the sea ice near pond inlet. *Polarforschung*, 44:117–126, 1974.

[35] P. Wong. The statistical physics of sedimentary rocks. *Physics Today*, 41(12):24–32, 1988.

[36] Jiayun Zhou, Bruno Delille, Hajo Eicken, Martin Vancoppenolle, Frédéric Brabant, Gauthier Carnat, Nicolas-Xavier Geilfus, Tim Papakyriakou, Bernard Heinesch, and Jean-Louis Tison. Physical and biogeochemical properties in landfast sea ice (Barrow, Alaska): Insights on brine and gas dynamics across seasons. *Journal of Geophysical Research: Oceans*, 118(6):3172–3189, 2013.